Journal of
Synchrotron
Radiation

ISSN 0909-0495

Received 7 May 2012
Accepted 21 June 2012

# Development of a two-dimensional imaging system of X-ray absorption fine structure

**Misaki Katayama,[a] Koichi Sumiwaka,[a] Kazuhiro Hayashi,[a] Kazuhiko Ozutsumi,[a] Toshiaki Ohta[b] and Yasuhiro Inada[a]***

[a]Department of Applied Chemistry, Ritsumeikan University, Kusatsu 525-8577, Japan, and [b]SR Center, Ritsumeikan University, Kusatsu 525-8577, Japan. E-mail: yinada@fc.ritsumei.ac.jp

A two-dimensional imaging system of X-ray absorption fine structure (XAFS) has been developed at beamline BL-4 of the Synchrotron Radiation Center of Ritsumeikan University. The system mainly consists of an ionization chamber for $I_0$ measurement, a sample stage, and a two-dimensional complementary metal oxide semiconductor (CMOS) image sensor for measuring the transmitted X-ray intensity. The X-ray energy shift in the vertical direction, which originates from the vertical divergence of the X-ray beam on the monochromator surface, is corrected by considering the geometrical configuration of the monochromator. This energy correction improves the energy resolution of the XAFS spectrum because each pixel in the CMOS detector has a very small vertical acceptance of $\sim$0.5 μrad. A data analysis system has also been developed to automatically determine the energy of the absorption edge. This allows the chemical species to be mapped based on the XANES feature over a wide area of 4.8 mm (H) $\times$ 3.6 mm (V) with a resolution of 10 μm $\times$ 10 μm. The system has been applied to the chemical state mapping of the Mn species in a $LiMn_2O_4$ cathode. The heterogeneous distribution of the Mn oxidation state is demonstrated and is considered to relate to the slow delocalization of $Li^+$-defect sites in the spinel crystal structure. The two-dimensional-imaging XAFS system is expected to be a powerful tool for analyzing the spatial distributions of chemical species in many heterogeneous materials such as battery electrodes.



**Keywords: imaging XAFS; two-dimensional detector; chemical state mapping; Li ion secondary battery; transmission mode.**

## 1. Introduction

The cathodes of lithium ion secondary batteries (LIBs) are generally manufactured from a mixture of an active material, a conductive additive and a polymer binder (Hassoun *et al.*, 2011). Since the secondary particles of the functional compounds in LIBs have sizes of the order of micrometers (Wilson *et al.*, 2011), the electrodes are heterogeneous on a micrometer scale. The chemical reactions are thus affected by the particle size and the surface condition of the electrodes (Kim *et al.*, 2009). The reaction has been reported to be inhomogeneous owing to temperature variation (Fleckenstein *et al.*, 2011) and physical tortuosity (Kehrwald *et al.*, 2011), which adversely affect the battery performance. It is thus critical to realise the inhomogeneity of active species and chemical reactions to greatly improve battery performance.

Chemical speciation is fundamental to clarifying chemical function and reactivity. Spatially resolved mapping of chemical speciation is very important, especially for heterogeneous samples that are chemically inhomogeneous. Scanning X-ray microscopy techniques have progressed greatly in the last 30 years (Sakdinawat & Attwood, 2010), and nanometer spatial resolution has been reached. X-ray fluorescence analysis has been used for performing spatially resolved mapping by using an X-ray microbeam. It has been widely used for investigating industrial chemical processes and biochemical samples. Fluorescence X-rays are generated by elements at the X-ray irradiation point and are detected by an energy-dispersive detector. The irradiation point of the X-ray microbeam is scanned by moving the sample to achieve two-dimensional mapping. Because the spatial resolution is limited by the size of the X-ray beam, much effort has been expended in reducing the X-ray beam size.

X-ray fluorescence analysis using an X-ray microbeam is very effective for determining the spatial distribution of an element. In addition, it is possible to analyze the chemical state of a specific element by scanning the energy of the incident X-ray microbeam to obtain a fluorescence XAFS spectrum of the irradiation position. Fluorescence XAFS spectroscopy can be used to determine the electronic state and local structure of a specific element, which is very important for understanding the chemical behavior of the element. Two-

dimensional imaging of XAFS spectroscopy can be performed by using an X-ray microbeam and detecting the fluorescence yield with the spatial resolution of X-ray microbeam size. However, many scans are required at different sample positions to generate an imaging map. It thus takes a very long time to obtain an imaging map, even when a strong X-ray source is utilized at a synchrotron radiation facility. The sample must be chemically stable during such measurements. Consequently, it is impractical to scan areas larger than the $mm^2$ order.

XAFS spectroscopy is the most useful analysis tool for investigating the cathode reaction of LIBs because the X-ray absorption near-edge structure (XANES) profile and the absorption-edge energy depend on the oxidation state of the transition metal element in the active material. XAFS spectroscopy has the great advantage that it can be used *in situ* to analyze electrode reactions. It is important to understand the chemical reactions that occur in batteries in order to develop next-generation secondary batteries. However, XAFS measurements in the transmission mode are generally unsuitable for *in situ* analysis of electrodes since they require samples with uniform concentrations and thicknesses. Two-dimensional imaging of fluorescence XAFS by using an X-ray microbeam has the potential to overcome this problem because its spatial resolution is sufficiently high to ascertain the expected inhomogeneity of the electrode (Kemner *et al.*, 2004). However, it is limited to a small scanning area, and the extremely high flux density of the X-ray microbeam may damage samples. Furthermore, the scanning of the sample makes it difficult to determine the measurement time at each position, which is a serious problem for time-resolved measurements of fast reactions.

A two-dimensional-imaging XAFS system with a two-dimensional detector has been previously reported for measuring transmitted (Rau *et al.*, 2003; Grunwaldt *et al.*, 2006) or fluorescence X-rays (Eba & Sakurai, 2005). The latter can monitor surface species, but the two-dimensional detector needs to be close to the sample surface to realise spatially resolved measurements because of the diverging fluorescence. It is thus not suitable for *in situ* measurements of LIB electrodes because they are contained in a cell jacket to protect them from air and moisture. The present study seeks to realise two-dimensional XAFS imaging in transmission mode that can be used for *in situ* analysis of LIBs. We have constructed a system at beamline BL-4 of the Synchrotron Radiation Center of Ritsumeikan University, which has a high flux, a parallel beam with a flat intensity distribution, and a large beam size. Although the system concept is almost identical to previous works (Rau *et al.*, 2003; Grunwaldt *et al.*, 2006), we have established a more general system in this study by introducing an energy correction procedure. Because the X-ray energy is distributed in the vertical direction owing to the diverging beam at the monochromator surface, an auto-correction algorithm to calibrate the energy shift has also been developed. It gave a higher energy resolution than conventional XAFS measurements. This paper reports the details of these measurements and the data-processing systems.

## 2. Two-dimensional-imaging XAFS system

An XAFS imaging system was constructed in the experimental hutch of the XAFS beamline BL-4 of the Synchrotron Radiation Center of Ritsumeikan University (Ozutsumi & Handa, 2004). BL-4 mainly consists of a Golovchenko-type double-crystal monochromator and Be windows to separate the vacuum chamber from the atmosphere. A Si(220) crystal is usually used as the monochromator at BL-4. White X-rays generated from a synchrotron light source travel to the experimental hutch without passing through any focusing optics. The horizontal and vertical X-ray acceptances are 3.5 mrad and 1.5 mrad, respectively; thus, the full beam size is about 17 mm × 7 mm at the sample position in the experimental hutch.

Fig. 1 shows a schematic diagram of the newly developed system. A monochromatic X-ray beam ejected from the Be window passes through an ionization chamber for $I_0$ measurements and reaches the sample, which is set on a remote-controlled *XZ* stage. The transmitted X-ray intensity is then detected by a two-dimensional X-ray detector (Flash2.8, Hamamatsu Photonics). The two-dimensional detector consists of a complementary metal oxide semiconductor (CMOS) image sensor, a zooming optics for visible light, and a scintillator. A P43 ($Gd_2O_2S:Tb^{3+}$) scintillator was used to convert X-rays to visible light. Because the detection efficiency and the spatial resolution depend on the scintillator thickness and material, the scintillator (10 μm thickness, Hamamatsu Photonics) deposited on a fiber optic plate can be replaced, enabling the optimal scintillator for XAFS imaging to be used. The zooming optics expands the image at the scintillator with a fixed expansion ratio of 1.45. The scintillator and the zooming optics were located in a box to shield them from visible light. This box has an X-ray window of aluminium-deposited Mylar film. The image sensor has 1920 × 1440 CMOS elements and the actual size of one element is 3.63 μm

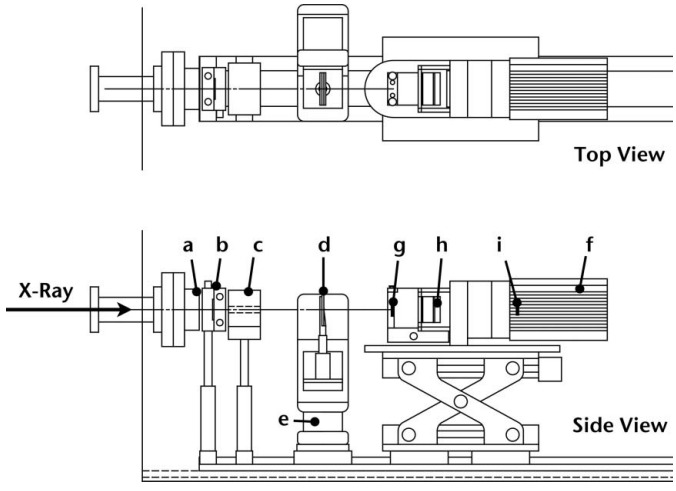


**Figure 1**
Schematic diagram of the two-dimensional XAFS imaging system. (*a*) Be window, (*b*) slit, (*c*) ionization chamber, (*d*) sample, (*e*) *XZ* stage, (*f*) two-dimensional detector, (*g*) scintillator, (*h*) zooming optics, (*i*) CMOS sensor.

× 3.63 μm. Thus, the field of view extends over an area of 4.8 mm × 3.6 mm with an ideal spatial resolution of 2.5 μm × 2.5 μm. The actual resolution is about 10 μm on the basis of a slit edge profile, which depends on the antiparallel ingredients of X-ray beams and the distance between the sample and the detector. The A/D converter of the image sensor has a 12-bit dynamic range.

The incident X-ray energy was varied by stepping the monochromator angle and the images obtained at different energies were transferred to a computer. XAFS spectra were then obtained from the transmitted X-ray images by dividing $I_0$ by the intensities measured at each X-ray energy. The background intensities are subtracted prior to calculating the absorbance. $I_0$ is usually taken to be the intensity measured by the ionization chamber to achieve a simple and quick XAFS measurement. The intensities measured using the two-dimensional detector for another energy scan without a sample can be used as $I_0$, and such a scan is necessary to perfectly remove the irregular features due to the glitch in $I_0$. Because the X-ray beam has an almost homogeneous intensity distribution, the intensity measured at a position where there is no sample can also be used as $I_0$; in this case there is negligible change in the intensity between scans.

## 3. Two-dimensional imaging of XAFS spectra and energy correction

A set of raw data obtained from a two-dimensional-imaging XAFS measurement consists of a three-dimensional array of the transmitted X-ray intensities, $I(E', x, y)$, where $E'$ is the apparent X-ray energy calculated by the angle of the monochromator and $(x, y)$ is the measurement position on the sample. The X-ray absorbance $\mu t$ at each position $(x, y)$ is expressed by (1),

$$\mu t(E', x, y) = \ln\big[I_0(E', x, y)/I(E', x, y)\big]. \quad (1)$$

When the incident X-ray intensities are measured by the ionization chamber, the $I_0(E', x, y)$ term is replaced by the detected value at $E'$. The XAFS spectrum for a specific area can be obtained by integrating $\mu t(E', x, y)$. However, because the energy of the incident X-ray beam varies vertically, it is necessary to convert the apparent X-ray energy $E'$ into the actual energy $E$ measured by one CMOS element. The incident angle to the monochromator crystal surface depends on the distance $(y)$ from the horizontal plane. When the angle between the monochromator crystal surface and the horizontal plane is $\theta$, the difference $(\Delta\theta)$ between the real incident angle and $\theta$ is geometrically derived at $y$ by the following equations for a Golovchenko-type monochromator,

$$\Delta\theta = \tan^{-1}\big[(y - y_0)/L\big], \quad (2)$$

$$L = L_0 + (D/\sin 2\theta) - (D/\tan 2\theta), \quad (3)$$

where $y_0$ denotes the vertical position of the horizontal plane, $L$ is the distance from the light source to the detector, $L_0$ corresponds to $L$ when $\theta = 45^\circ$, and $D$ is the height difference

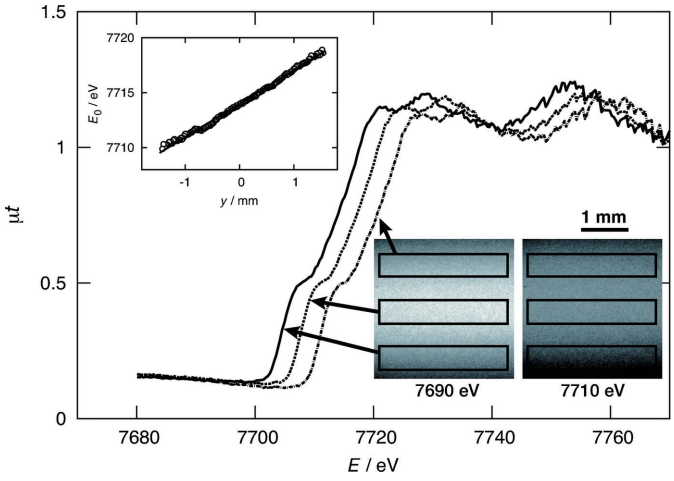


**Figure 2**
Energy shift of XANES spectra of a Co foil by the position in the X-ray beam. The observed X-ray energy ($E_0$) of the absorption edge for each detector line is plotted *versus* vertical position ($y$) in the inset. Two transmitted X-ray images measured at around the absorption-edge energy are presented.

of the X-ray beams before and after the monochromator. The actual X-ray energy, $E$ (eV) at position $y$ is then given by

$$E = 12398.52/[2d\sin(\theta + \Delta\theta)], \quad (4)$$

where $d$ (Å) is the lattice spacing of the monochromator crystal. Fig. 2 shows XAFS spectra of a Co foil measured using the newly developed two-dimensional-imaging XAFS system. A plot of $\mu t$ values at three different areas is given in Fig. 2 as a function of the apparent $E'$ value. It clearly shows that the absorption edge is different in the three spectra and that the edge energy in the upper area is higher than that in the lower area. The observed X-ray energy ($E_0$) of the absorption edge is plotted as a function of $y$ in the inset of Fig. 2; it is well reproduced by (2)–(4). It is thus found that the actual energy $E$ can be reasonably corrected by introducing the term $\Delta\theta$. This geometrical correction is applicable to any $\theta$, because the concept of (2)–(4) is independent of $\theta$.

We have developed an analysis program for automatically correcting the energy shift and for analyzing the spectra at all the detector elements. The absorption edge energy, $E_0$, can be automatically obtained from the maximum of the first derivative of $\mu t$. The chemical state of the absorbing element is judged on the basis of $E_0$. In addition, the contents of absorbing elements can be determined from the absorbance difference, $\Delta\mu t$, between the pre- and post-edge regions. The analysis program can generate two-dimensional maps of the chemical state of absorbing elements by varying the color and the brightness according to the $E_0$ and $\Delta\mu t$ values.

## 4. High-energy resolution for conventional XAFS measurements

The energy resolution $(\Delta E/E)$ is mainly determined by the vertical opening of the slit, which is usually located downstream of the monochromator for the conventional XAFS

measurement system with ionization chambers, and is represented by the following equations,

$$\Delta E/E = \left(\omega^2 + \varphi^2\right)^{1/2} \cot\theta, \tag{5}$$

$$\varphi = 2\tan^{-1}\left[(b + \sigma_v)/2l\right], \tag{6}$$

where $\omega$ is the diffraction angle width of the monochromator crystal [$\omega$ = 0.024 mrad at 8 keV for Si(220)], $\varphi$ is a parameter that depends on the beamline conditions and the light source as expressed by (6), $\sigma_v$ is the vertical size of the synchrotron light source (140 µm in the case of the Synchrotron Radiation Center of Ritsumeikan University), and $b$ is the opening width of the slit at a distance $l$ from the light source (it is normally set to 1.0 mm for $l$ = 5000 mm). For the newly developed two-dimensional-imaging XAFS system the value of $b$ is replaced by the vertical spatial resolution of the detection system (2.5 µm), which is considerably smaller than $\sigma_v$. Each pixel in the CMOS detector has a very small vertical acceptance of $\sim$0.5 µrad. Spectra with a high energy resolution are thus obtained by integrating the data of all the detector lines after correcting for the energy shift in the manner described above. Because the energy values at each detector line differ owing to the energy correction procedure, the energy is interpolated for the integration. The highest energy resolution was achieved by using the two-dimensional detector at beamline BL-4. A shoulder structure of the absorption edge is clearly seen in the XANES spectrum obtained using the two-dimensional detector, as shown in Fig. 3, in which the XANES spectra of a Co foil are compared. The spectrum of the conventional measurement using two ionization chambers (Fig. 3*b*) was measured at the standard setting of BL-4, and its energy resolution is poor owing to the large vertical acceptance to gain the X-ray flux in the case of BL-4. The two-dimensional detector is found to give a high energy resolution for conventional XAFS measurements of a homogeneous sample.

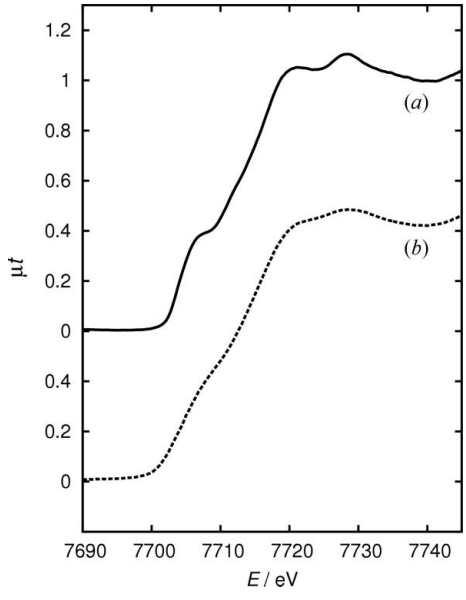


**Figure 3**
Improvement of energy resolution for a Co foil by correcting the energy shift. (*a*) Two-dimensional detector, (*b*) conventional measurement using ionization chambers.

## 5. Application to a LIB cathode sample

The two-dimensional XAFS imaging system was used to analyze chemical species distributions on a LIB cathode material. Lithium manganese oxide ($LiMn_2O_4$) is a promising material for next-generation LIBs. $LiMn_2O_4$ has a spinel crystal structure and higher stability than $LiCoO_2$; however, it has the problem of a capacity drop with repeating charging/discharging cycle. Various attempts were examined to improve the charging/discharging cycle property of the rechargeable battery, such as the doping of lanthanide ions (Sun *et al.*, 2012) and transition metal ions (Sung *et al.*, 2008). We thus applied the developed two-dimensional-imaging XAFS system to obtain the XAFS imaging maps at the Mn *K*-edge of an actual $LiMn_2O_4$ cathode sample.

$LiMn_2O_4$ was synthesized by the solid-phase method reported previously (Xia *et al.*, 1995). A cathode was made from a mixture of $LiMn_2O_4$ powder, acetylene black and polyvinylidene difluoride. A lithium ion battery cell was assembled using the cathode, lithium foil as the anode, separator sheets, and 1 mol $dm^{-3}$ $LiPF_6$ solution dissolved in a mixture of ethylene carbonate and ethyl methyl carbonate in a glove box. The observed battery capacity (120 mA h $g^{-1}$) was confirmed to be close to the theoretical value (148 mA h $g^{-1}$) after an aging procedure of three charging/discharging cycles. The 50%-charged cell was disassembled under an inert atmosphere, and the washed and dried cathode sample was analyzed by the two-dimensional-imaging XAFS system.

Fig. 4 shows an example of an XAFS imaging map of the Mn species. The absorption-edge energy is shifted to higher energies by charging the LIB, because the charging process increases the proportion of Mn(IV) species. In Fig. 4 the blue and red pixels indicate the regions containing the lower [Mn(III, IV)] and higher oxidation states [Mn(IV)], respectively. The yellow pixels indicate regions where the absorption-edge energy is intermediate between them. Heterogeneous mixing of the Mn(III, IV) and Mn(IV) species is clearly observed in Fig. 4 at the 50%-charged state, and the ratio of the blue and red pixels is almost in agreement with the charging percentage. The heterogeneous distribution between the charged and discharged states can indicate that the delocalization of $Li^+$-defect sites is slow for the $LiMn_2O_4$ cathode with the spinel crystal structure. The slow relaxation for $LiMn_2O_4$ will be contrasted with further measurements of other cathode materials, such as $LiCoO_2$ and $LiNiO_2$ with a layered rock salt structure.

## 6. Conclusion

A two-dimensional XAFS imaging system has been newly developed at beamline BL-4 of the Synchrotron Radiation Center of Ritsumeikan University. The X-ray energy shift originating from the vertical divergence of the X-ray beam is corrected based on the geometrical configuration of the

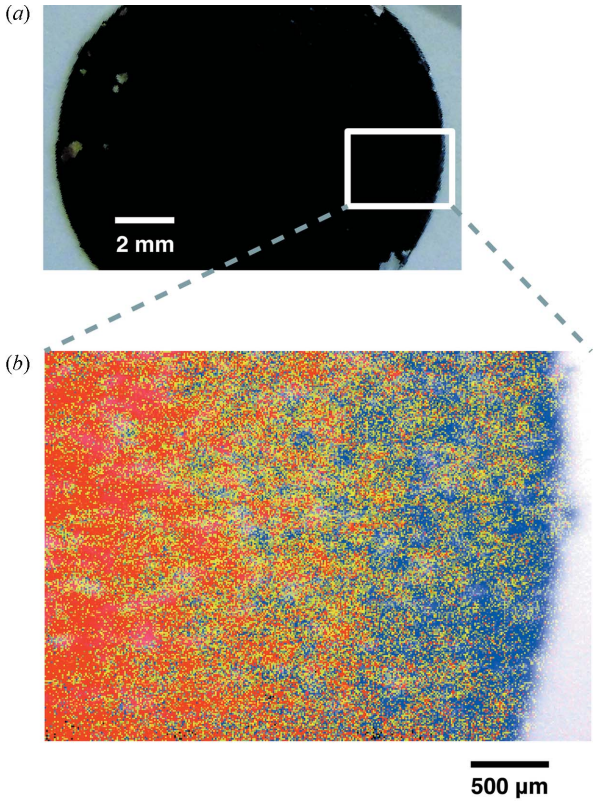


**Figure 4**
Optical (*a*) and XAFS (*b*) images for the $LiMn_2O_4$ cathode sample of LIB at the 50%-charged state. The Mn species with lower and higher oxidation states are depicted by blue and red pixels, respectively, in (*b*).

monochromator. The chemical state of X-ray absorbing atoms over an area of a few $mm^2$ can be analyzed by the two-dimensional-imaging XAFS system with an actual spatial resolution of 10 µm × 10 µm. When the two-dimensional detector is applied to a homogeneous sample, the obtained XAFS spectra have a higher energy resolution than those of conventional transmission measurements using ionization chambers at BL-4 owing to the small vertical acceptance of the detector elements. Chemical state mapping of the Mn species in an actual LIB electrode was performed for a $LiMn_2O_4$ cathode. XAFS imaging revealed for the first time that the Mn oxidation state has a heterogeneous distribution in a 50%-charged cathode. The inhomogeneity can be related to the slow delocalization of $Li^+$-defect sites in the spinel crystal structure. Microscopic speciation for the transient electrode during the charging/discharging process will be very useful for creating the next-generation materials for rechargeable batteries.

This work was partially supported by the Research and Development Initiative for Scientific Innovation of New Generation Battery (RISING) project from the New Energy and Industrial Technology Development Organization (NEDO), Japan.

## References

Eba, H. & Sakurai, K. (2005). *Chem. Lett.* **34**, 872–873.
Fleckenstein, M., Bohlen, O., Roscher, M. A. & Bäker, B. (2011). *J. Power Sources*, **196**, 4769–4778.
Grunwaldt, J. D., Hannemann, S., Schroer, C. G. & Baiker, A. (2006). *J. Phys. Chem. B*, **110**, 8674–8680.
Hassoun, J., Lee, K. S., Sun, Y. K. & Scrosati, B. (2011). *J. Am. Chem. Soc.* **133**, 3139–3143.
Kehrwald, D., Shearing, P. R., Brandon, N. P., Sinha, P. K. & Harris, S. J. (2011). *J. Electrochem. Soc.* **158**, A1393–A1399.
Kemner, K. M., Kelly, S. D., Lai, B., Maser, J., O'loughlin, E. J., Sholto-Douglas, D., Cai, Z., Schneegurt, M. A., Kulpa, C. F. & Nealson, K. H. (2004). *Science*, **306**, 686–687.
Kim, K. M., Lee, S. H., Kim, S. & Lee, Y.-G. (2009). *J. Appl. Electrochem.* **39**, 1487–1495.
Ozutsumi, K. & Handa, K. (2004). *Rev. Sci. Instrum.* **75**, 111–118.
Rau, C., Somogyi, A. & Simionovici, A. (2003). *Nucl. Instrum. Methods Phys. Res. B*, **200**, 444–450.
Sakdinawat, A. & Attwood, D. (2010). *Nat. Photon.* **4**, 840–848.
Sun, H., Chen, Y., Xu, C., Zhu, D. & Huang, L. (2012). *J. Solid State Electrochem.* **16**, 1247–1254.
Sung, N.-E., Sun, Y.-K., Kim, S.-K. & Jang, M.-S. (2008). *J. Electrochem. Soc.* **155**, A845–A850.
Wilson, J. R., Cronin, J. S., Barnett, S. A. & Harris, S. J. (2011). *J. Power Sources*, **196**, 3443–3447.
Xia, Y., Takeshige, H., Noguchi, H. & Yoshio, M. (1995). *J. Power Sources*, **56**, 61–67.